Surface & Coatings Technology 261 (2015) 141–148

Contents lists available at ScienceDirect

Surface & Coatings Technology

journal homepage: www.elsevier.com/locate/surfcoat

Influence of SiO_2 nanoparticles on hardness and corrosion resistance of electroless Ni–P coatings

Mohammad Islam [a,*], Muhammad Rizwan Azhar [b], Narjes Fredj [c], T. David Burleigh [c], Olamilekan R. Oloyede [d,e], Abdulhakim A. Almajid [f], S. Ismat Shah [g]

[a] Center of Excellence for Research in Engineering Materials (CEREM), Advanced Manufacturing Institute, King Saud University, P.O. Box 800, Riyadh 11421, Saudi Arabia
[b] Chemical Engineering Department, Curtin University, Bentley 6102, WA, Australia
[c] Materials and Metallurgical Engineering Department, New Mexico Institute of Mining and Technology, Socorro, NM 87801, USA
[d] Institute for Materials Research (IMR), School of Chemical & Process Engineering, Faculty of Engineering, University of Leeds, UK
[e] Maritime Academy of Nigeria, Oron, Nigeria
[f] Department of Mechanical Engineering, King Saud University, P.O. Box 800, Riyadh 11421, Saudi Arabia
[g] Department of Materials Science & Engineering, University of Delaware, Newark, DE 19716, USA

ARTICLE INFO

Article history:
Received 1 May 2014
Accepted in revised form 18 November 2014
Available online 29 November 2014

Keywords:
Nanocomposite Coatings
Electroless
Electrochemical Impedance Spectroscopy
Ni-P-SiO_2
Hardness

ABSTRACT

Nickel–phosphorus (Ni–P) coatings with controllable P content and desirable characteristics can be produced by tuning bath chemistry and processing conditions during the electroless process. Although pure medium- and high-P coatings offer a good combination of mechanical and corrosion properties, their performance attributes can be further enhanced through incorporation of silica (SiO_2) nanoparticles. Using 15 and 30 g/L of sodium hypophosphite as reducing agent in the plating bath, Ni–P coatings with respective P content of 10.8 and 14.3 wt.% were produced. While the surface roughness and grain size increased with an increase in the P content, the average hardness value and corrosion resistance of medium-P coatings were superior to their high-P counterparts. The average hardness of the Ni–P– SiO_2 coatings based on medium-P Ni–P matrix was determined to be ~11.0 GPa. Electrochemical impedance spectroscopy (EIS) studies of these coatings indicated area-impedance values on the order of $10^8\ \Omega\cdot cm^2$, whereas the double-layer capacitance per unit area (C_{dl}) and charge transfer area-resistance (R_{ct}) values, computed from theoretical fit of the EIS data, were in the range of $1.18\times10^{-10}\ F\cdot cm^{-2}$ and $3.14\times10^8\ \Omega\cdot cm^2$, respectively. The findings confirmed that addition of SiO_2 nanoparticles modifies deposit morphology through grain refinement, reduction in the surface roughness and minimization of surface porosity in the nanocomposite coatings.

1. Introduction

The electroless deposition process can be employed to produce pure nickel–phosphorus (Ni–P) alloy coatings as well as nanocomposite coatings that offer strong potential for use in structural and functional applications [1,2]. Several factors including substrate pre-treatment, plating bath composition, temperature, pH, agitation, heat treatment, etc. strongly influence deposit characteristics such as growth rate, composition, morphology and physical properties [3–9]. An essential component of the precursor bath is the reducing agent that acts as a continuous source of electrons for reduction of cations in the solution. Among several choices, sodium hypophosphite (NaH_2PO_2) is the most commonly used reducing agent in the plating bath. It is also a source of P in the resulting deposit which gets codeposited along with nickel from the solution. Thus, the amount of reducing agent dictates P content in the coatings, which can be categorized as (by weight percent) low- (1–5%), medium- (6–9%) or high-P (≥10%) coatings with a maximum amount of ~17 wt.%. Generally, medium- and high-P coatings exhibit an excellent combination of wear and corrosion resistance [10].

Incorporation of uniformly distributed second-phase particles or nanostructures into the electroless Ni–P coatings has strong potential for diverse applications due to the enhancement of tribological properties and corrosion resistance via improvements in coating characteristics and dispersion hardening [11]. Uniform distribution of the second phase particles into the metallic matrix is ensured by magnetic agitation, stirring, sonication and/or particle surface modification using an appropriate surfactant to avoid flocculation, particularly in case of nanostructures. Several studies have reported the effect of micro- and nanometer size particle incorporation (such as Al_2O_3, CNTs, SiC, SiO_2, TiO_2, ZrO_2, etc.) on the corrosion resistance and tribological behavior of the composite coatings [12–17]. The particle incorporation into the growing coating is accomplished through a number of steps namely,

* Corresponding author. Tel.: +966 11 467 0760 (work); fax: +966 11 467 0199.
E-mail addresses: mohammad.islam@gmail.com, miqureshi@ksu.edu.sa (M. Islam), rizwanazharr@yahoo.com (M.R. Azhar), nfredj@nmt.edu (N. Fredj), burleigh@nmt.edu (T.D. Burleigh), pmoro@leeds.ac.uk (O.R. Oloyede), aalmajid@ksu.edu.sa (A.A. Almajid), ismat@udel.edu (S. Ismat Shah).

http://dx.doi.org/10.1016/j.surfcoat.2014.11.044
0257-8972/

possible particle surface modification, particle transportation initially through convection and subsequently by diffusion, migration across an electrical double layer and physical embedding. Furthermore, process parameters related to particle characteristics, bath composition, flow environment and substrate condition strongly influence the deposit properties in terms of particle content, coating surface roughness and morphology, void fraction and hardness. The development of metal matrix composite coatings and chronological evolution of mathematical models to correlate plating conditions with coating characteristics were recently described by Walsh and Leon [18].

Due to a low value of Hamakar constant (1.6 in water) and the tendency to form hydration layers that inhibit agglomeration of nanoparticles, SiO_2 can be used at small loading levels to produce Ni–P–SiO_2 nanocomposite coatings [19]. Upon addition into the Ni–P coating matrix, the SiO_2 particles are believed to hinder dislocation movement, thus acting as a barrier to plastic deformation of the ductile matrix. The maximum degree of SiO_2 incorporation into Ni–P coatings is ~25 vol.% for 10 g/L of SiO_2 nanoparticles in the bath [20]. The SiO_2 nanoparticles have been reported to maximize microhardness and minimize wear rate upon heat treatment of the composite coatings [21]. Gutsev et al. [22] have reported that addition of nanosize SiO_2 improves wear resistance at low loads and in the case of steel counter-body. For aluminum substrates, the effect of SiO_2 nanoparticle content in the Ni–P–SiO_2 coatings on the corrosion resistance has been investigated [23]. A bath loading of 7 g/L SiO_2 led to ~2 wt.% SiO_2 addition in the composite coating with improvement in the corrosion resistance in the salt solution [24].

Although there is research literature available on the electroless Ni–P–SiO_2 nanocomposite coatings, there is a lack of a systematic study investigating the effect of SiO_2 addition on the corrosion resistance using EIS for prolonged exposure to salt solution. In this paper, we investigate the effect of sodium hypophosphite and relatively small amounts of SiO_2 nanoparticle content in the plating bath on the morphology and composition, hardness and corrosion properties of the Ni–P based coatings. Unlike many studies, use of small SiO_2 loading levels in the precursor bath facilitates dispersion without any need for an appropriate surfactant, thus keeping the bath chemistry relatively less complicated. First, Ni–P coatings with medium- and high-P content were produced and characterized. Due to superior corrosion resistance of the medium-P coatings, the effect of SiO_2 nanoparticle addition into these coatings was assessed using EIS technique.

2. Experimental procedures

For this work, analytical grade chemicals (Sigma Aldrich, purity ≥ 99.5%) were used as-received and without any further treatment. The aqueous solution for electroless deposition was prepared from certain amounts of nickel chloride ($NiCl_2$), sodium hypophosphite (NaH_2PO_2), sodium succinate ($C_4H_4Na_2O_4$), and sodium chloride (NaCl) with their respective roles as precursor chemical reagents for Ni^{2+} ions, reducing agent, complexing agent and surface activation.

The copper coupons (99.9% purity; 2.54 × 2.54 cm^2 in size) were ground with different SiC papers and then polished with 1 μm diamond paste. The samples were cleaned with isopropanol to remove any residue from the polishing fluid and rinsed with distilled water. Immediately after cleaning, substrates were immersed into the solution at 90 °C for different times in order to produce pure Ni–P or Ni–P–SiO_2 coatings.

For nanocomposite coatings, a pre-coat of Ni–P coating with the same composition was applied. An aqueous suspension of SiO_2 nanoparticles (Aldrich, 10–20 nm, 99.5%) was made through ultrasonic dispersion of the nanoparticles for 30 min followed by addition to the electroless plating bath. During pre-coat as well as nanocomposite deposition process, the solution was magnetically stirred at 50 rpm to ensure continuous supply of metal ions and SiO_2 nanoparticles initially at the substrate surface and later at the coating growth front. It should be noted, however, that controlling bath hydrodynamics is a challenge when addressing scale-up issues and other more effective bath agitation approaches must be explored. After deposition, the samples were thoroughly rinsed with the distilled water. Table 1 lists sample identification scheme and deposition conditions for pure and composite coatings.

The coatings were examined for surface topography and microstructure using a field-emission scanning electron microscope (FE-SEM) (JEOL; JSM7600F) by operating at 5 kV with 4.5 mm of working distance for good image resolution. The energy dispersive spectrum (EDS) analysis of the coatings was performed using Oxford Instruments X-act detector. The atomic force microscope (Park Systems, XE-100) was operated in the contact mode for three-dimensional surface topography of the coatings with contact cantilever (PPP-CONTSCR). For microhardness measurement, a nanoindentation system (Micro Materials, NanoTest Vantage) with Berkovich indenter was used with depth control measurements at a maximum load of 20 mN. The sample was mounted on the stub using cyanoacrylate adhesive and the average hardness values were computed from at least 10 indentation tests for each sample.

The corrosion studies were performed by electrochemical impedance spectroscopy (EIS) in 4 wt.% NaCl salt solution. The coating surface, a saturated calomel electrode (SCE) and a platinum electrode were employed in a three-electrode configuration as the working electrode, the reference electrode and the counter electrode, respectively, through connection with the Autolab Potentiostat (PGSTAT20 computer controlled). The measurements were made at open circuit potential from 10 mHz to 1 or 10 kHz with an AC wave of ±5 mV (peak-to-peak) overlaid on DC biased potential, and impedance data were collected at ten points per decade. The corrosion data was analyzed using NOVA 1.8 software. Samples were tested for different immersion times and after each EIS measurement, were kept immersed into NaCl solution with glass beakers covered with aluminum foil to avoid evaporation. Also, multiple samples of the same composition were tested to assess reproducibility of the data. Despite the main advantage of EIS being a non-destructive testing technique that produces time-dependent, quantitative data, it mostly provides a rapid indication of corrosion rates, thus underlining the importance of potentiodynamic polarization studies.

3. Results and discussion

3.1. Morphological and compositional characterization

The surface morphologies of the deposits at low and high magnification are presented in Fig. 1. The microstructures at low magnification reveal island growth mode of coating deposition with presence of large, spherical granules along with fine-grain structure. For sample 1 (Fig. 1a,b), the average grain size is on the order of ≤1 μm, while the large, round grains are few micrometers in size. As the NaH_2PO_2 content in the plating bath is increased from 15 to 30 g/L, the coating surface appears to be smoother with slightly larger grain size. From the weight change measurements, it is found that the deposition rate increases

Table 1
Processing conditions, composition and average hardness values for pure Ni–P and Ni–P–SiO_2 nanocomposite coatings.

ID	Synthesis conditions				Wt.	Coating comp. (wt.%)				Hardness
	NaH_2PO_2	SiO_2	Temp.	Time	(mg)					(GPa)
	g/L	g/L	°C	h		Ni	P	Si	O	
1.	15	×	90	1.5	23.9	89.2	10.8	×	×	4.42 ± 0.70
2.	30	×	90	1.5	100	85.7	14.3	×	×	3.15 ± 0.26
3.	15	1	90	2.0	60.3	85.8	8.90	2.30	3.22	10.07 ± 0.58
4.	15	2	90	2.0	41.8	85.5	8.82	2.42	3.19	11.0 ± 0.96
5.	30	1	90	2.0	40.0	77.0	17.1	2.07	3.82	5.69 ± 1.03
6.	30	2	90	2.0	35.2	77.0	17.2	2.39	3.33	6.46 ± 0.86

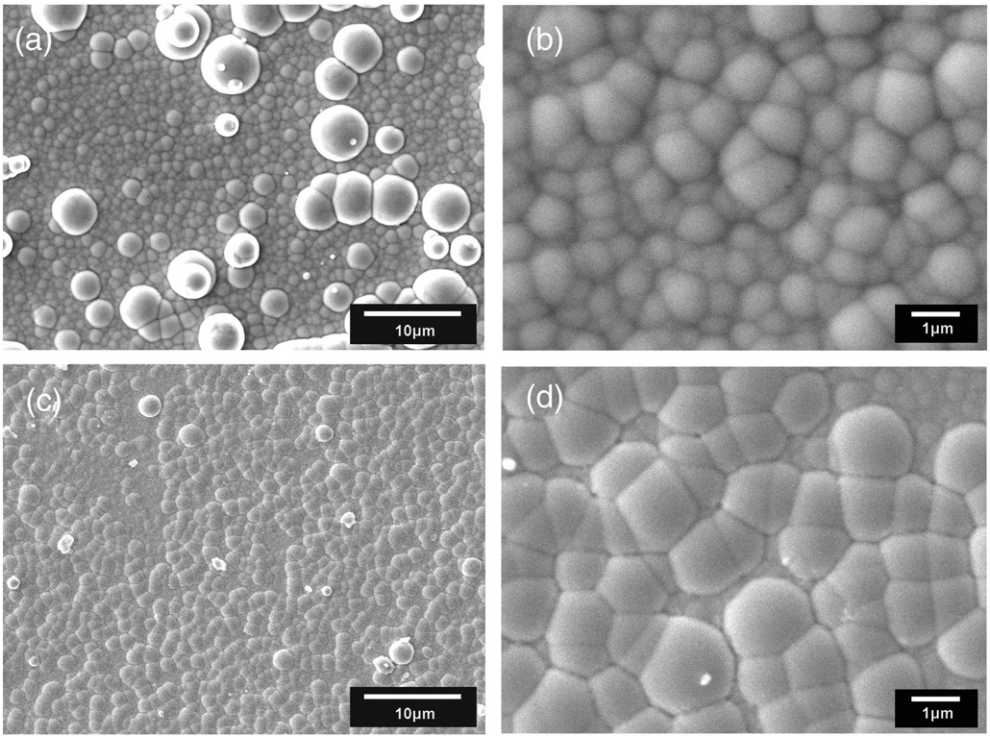

Fig. 1. Low and high magnification FE-SEM surface microstructures of pure Ni–P coatings: (a, b) sample 1 and (c, d) sample 2.

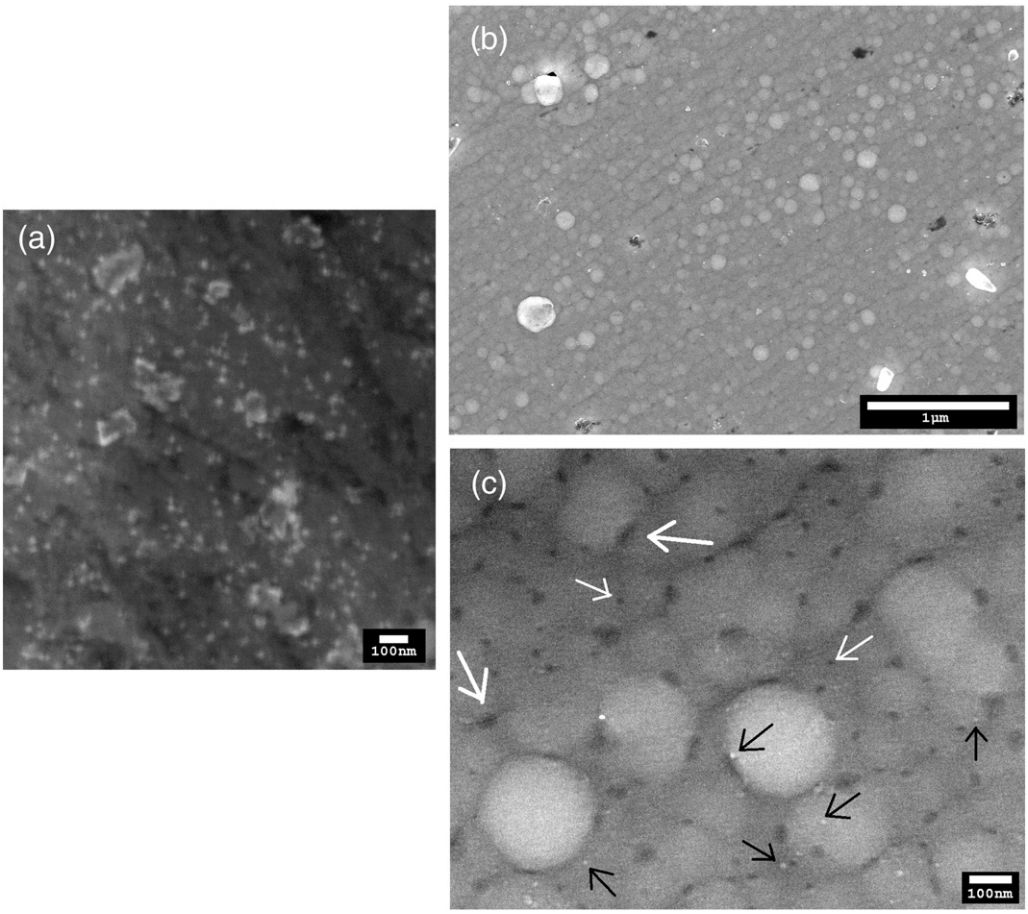

Fig. 2. (a) High magnification view of SiO_2 nanoparticles and (b, c) surface microstructure of Ni–P–SiO_2 coating (sample 6) showing surface morphology and nanoparticle dispersion.

upon increasing the NaH_2PO_2 content. The EDS analysis points to an associated increase in the P content from 10.8 to 14.3 wt.%. Table 1 lists weight gain and elemental composition (by weight percent) for the pure and nanocomposite coatings.

During growth of nanocomposite coatings, the particles are transported to the growth front via convective-diffusion followed by adsorption to the coating and subsequent irreversible incorporation due to reduction of the adsorbed Ni^{2+} and P^{3+} ions from $NiCl_2$ and NaH_2PO_2, respectively. The incorporation of SiO_2 nanoparticles (Fig. 2a) in the coating (sample 6) causes the surface microstructure to become very smooth, as shown in Fig. 2b. The added nanoparticles are believed to inhibit growth of the Ni–P nodules thus reducing their size to approximately 106 ± 3.7 nm, as estimated from Fig. 2b, besides a decrease in surface roughness and defect density which is in agreement with an earlier report [22]. High magnification view revealed presence of shallow black pores, indicated by white arrows in Fig. 2c, having diameters in the sub-100 nm size regime within and at the grain boundaries. The pores within grains are round (small arrows) with relatively smaller size of 15 nm or above, whereas elongated/elliptical shaped pores (pointed with thick arrows) with a few tens of nanometer diameters are observed at the grain boundaries. From Fig. 2c, the pore density was computed to be 0.76 μm^2. Some of the SiO_2 nanoparticles present in the coating are also visible as white round spots, as indicated by black arrows in Fig. 2c. The volume fraction of SiO_2 within Ni–P matrix is not expected to exceed 7% and does not exhibit a dramatic increase upon increasing the SiO_2 loading level in the bath from 1 to 2 g/L [20,22]. Nevertheless, such small amounts are sufficient to induce morphological changes in deposit characteristics. The EDS analysis confirms incorporation of SiO_2 nanoparticles besides an associated enhancement in the degree of P co-deposition to ~17 wt.% in the high-P deposits. The as-deposited coatings whether pure or nanocomposite are microcrystalline or amorphous with no distinct diffraction peaks (not shown).

From 20 × 20 and 1 × 1 μm area scans, the surface topographies of the Ni–P–SiO_2 nanocomposite coating (sample 4) are shown in Fig. 3. AFM results reveal the general morphological characteristics in terms of hemispherical grains and small perturbations representative of added nanoparticles on the nanocoating surface. Whereas fewer pores are visible on the nanocoating surface produced from less SiO_2 loading (1 g/L) in the bath, the three-dimensional microstructure confirms the presence of elongated/inter-connected pores at the boundaries of spherical nodules. The absence of any agglomerates from the nanocoating microstructures confirm uniform dispersion of nanoparticles in the Ni–P matrix, thus eliminating the need for a suitable surfactant that otherwise makes bath chemistry more complex. From cyclic voltammetry studies on electroless nickel coatings, the log–log relationship between coating thickness and percent porosity has been reported to be inverse linear [25]. From thickness values of the Ni–P–SiO_2 nanocoatings, the porosity is anticipated to be less than 2%. From AFM examination, the average surface roughness values (R_a) are found to decrease from 1.3 μm for the pure Ni–P coating to 45 nm for the Ni–P–SiO_2 nanocoatings, underlying the important role of nanoparticles towards modification of deposit morphology. Beside codeposition of nanoparticles on the coating front, surface modification of the nanoparticles present in colloidal state may also occur through surface activation and subsequent deposition by Ni–P deposit [26–29]. For small SiO_2 loading levels as in this work, it is anticipated that nanoparticle codeposition occurs uniformly over the coating. The nanoparticle surface activation while in the plating bath or after adsorption to the coating growth front may act as potential nucleation sites for further Ni–P deposition, thus causing grain refinement and minimization of porosity level in the nanocoatings.

The microstructure of the Ni–P–SiO_2 nanocomposite coating (sample 5) after 14 days of immersion in NaCl solution is presented in Fig. 4. From overall view of the surface, two distinctly different surface morphologies are evident. There are relatively smooth regions with

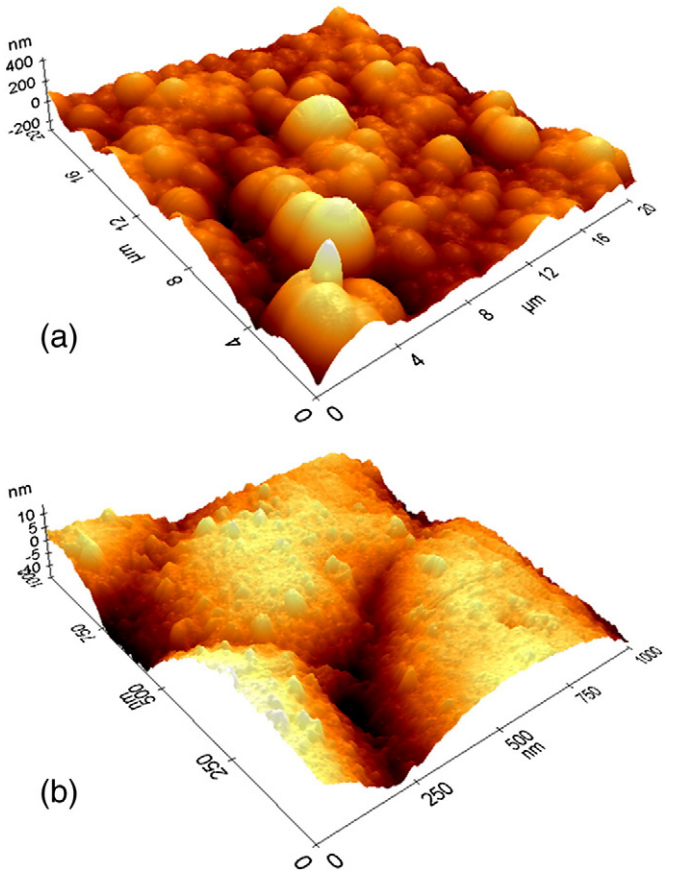

Fig. 3. (a) Three-dimensional surface topography of Ni–P–SiO_2 film surface (sample 4): (a) a large 20 × 20 μm area scan and (b) a small 1 × 1 μm area scan.

little or no change after corrosion tests and there are certain areas with rough morphology showing formation of fine cracks. At high magnification (Fig. 4b), the smooth area appears to be composed of fine grains that are about 25 nm in size besides the presence of few round surface pores. It is interesting to note that the pore size is in the same range as that of SiO_2 nanoparticles and, therefore, the pore formation maybe attributed to the detachment of individual SiO_2 nanoparticles from the surface. Nevertheless, observation of a predominantly defect-free, smooth surface after prolonged exposure is a testament to the fact that the presence of SiO_2 nanoparticles effectively inhibits corrosion in salt solution through surface passivation. The granular structure with size on the same scale, albeit with a high degree of surface roughness and surface cracks, is observed while examining the coarse area in Fig. 4a. From the microstructure (Fig. 4c), the surface cracks are estimated to be a few tens of nanometers wide with lengths on the order of few hundred nanometers. The cracks seem to have originated from large pores that were observed on the grain boundaries of the as-deposited Ni–P–SiO_2 coatings and became wider due to the cumulative effect of electrolyte penetration into pores while immersed and release of residual tensile stress from the as-deposited film [30]. The crack density is low in the nanocomposite coating and, although the cracks at the grain boundaries are relatively longer and wider, they are not deep enough to expose the substrate underneath and cause coating delamination. Therefore, under the corrosion testing conditions explored during this work, the nanocomposite coatings maintain their structural integrity.

3.2. Indentation studies

For polished copper substrate, the average hardness value was found to be 1.80 GPa. Fig. 5 represents data from 10 indentation tests performed

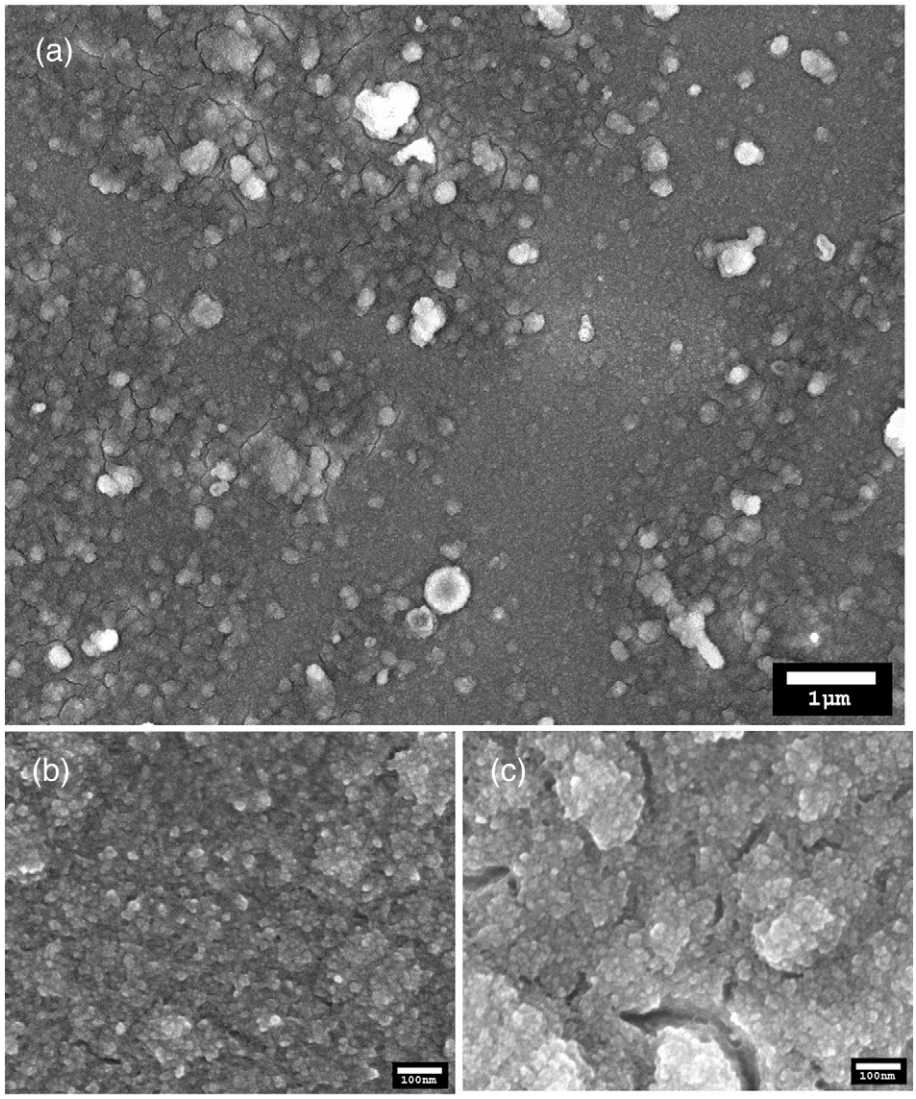

Fig. 4. (a) Microstructural examination of the nanocomposite coating (sample 5) after 14 days of immersion in NaCl solution: (a) Overall surface showing smooth and coarse areas, (b) high magnification view of the smooth surface and (c) coarse area showing small surface cracks.

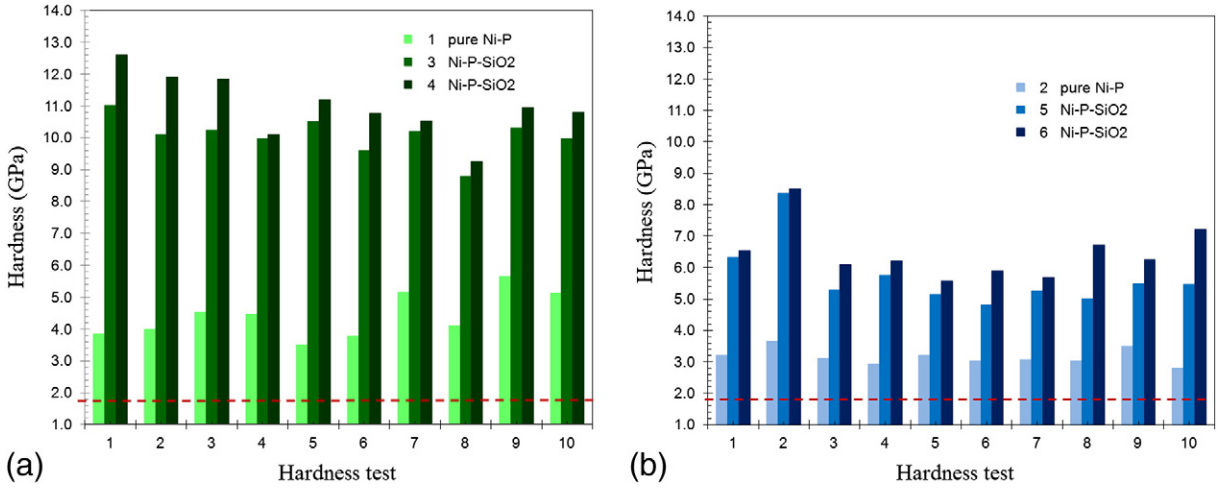

Fig. 5. Indentation data for pure Ni–P and Ni–P–SiO_2 nanocomposite coatings produced with (a) 1 g/L and (b) 2 g/L SiO_2 nanoparticle loading in the bath. The dashed line represents average hardness of the copper substrate.

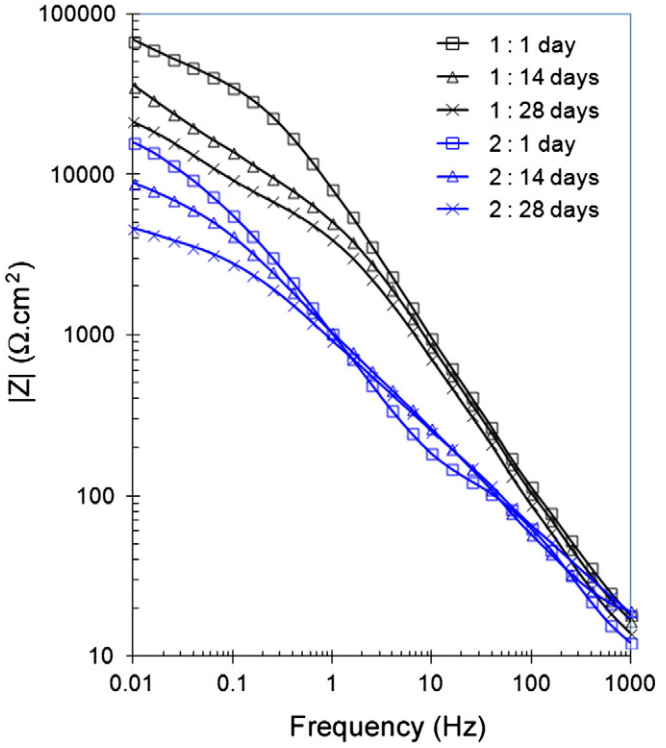

Fig. 6. Bode diagrams for pure Ni–P coatings (samples 1 and 2) from different immersion times in 4 wt.% NaCl solution.

on each sample after coating deposition as well as immersion in saline solution for a certain period. The average values are listed in Table 1. Comparison of pure Ni–P coatings with different P content reveals that Ni–P coating with less P (sample 1) exhibits higher hardness value of 4.42 GPa. The hardness value for SiO_2 in bulk form is 10.98 GPa [31]. For both Ni–P compositions, addition of SiO_2 causes an increase in the hardness value of the resulting nanocomposite coating with greater extent of increase noticed in coatings produced with 2 g/L SiO_2 in the bath. Two- to three-fold increase in hardness was recorded despite the fact that the coatings produced are a few microns thick and no post-deposition heat treatment was performed.

The incorporation of SiO_2 nanoparticles into the Ni–P matrix greatly enhances the overall hardness through modification of the coating morphology, in terms of more refined nodular structure with elimination of surface porosity, and by impeding the fast dislocation movement in the ductile matrix. For the same Ni–P coating composition, the average hardness value increases upon increasing the SiO_2 nanoparticles loading in the plating bath from 1 to 2 g/L, thus indicating greater degree of SiO_2 incorporation and subsequently more effective reinforcement of the metallic matrix. The scatter in data, as suggested by high standard deviation values for samples 4–6, maybe caused by non-uniform dispersion of SiO_2 nanoparticles and to a certain degree of agglomeration due to high surface area. Nevertheless, the values obtained are higher than those reported for similar nanocomposite coatings and are even comparable to their heat-treated counterparts in some cases [20,21].

3.3. EIS analysis

The corrosion studies of the pure Ni–P and nanocomposite Ni–P–SiO_2 coatings were carried out in 4 wt.% NaCl solution. The Bode plots and Nyquist charts for up to 28 days of immersion in salt solution are presented in Figs. 6 and 7, respectively. From area impedance data (Fig. 6), it is evident that pure alloy coating of the composition 89.2Ni–10.8P (sample 1) offers superior corrosion resistance than that of 85.7Ni–14.3P (sample 2) during the entire period of immersion in salt solution. In both cases, area-impedance values progressively decreased after longer immersion times indicating gradual structural deterioration of the coating. At low frequencies in the range of 10–100 mHz, the area-impedance drops upon extended exposure to saline solution, although sample 1 (89.2Ni–10.8P) exhibits superior corrosion resistance. The corresponding Nyquist plots for samples 1 and 2 are shown in Fig. 7 to represent the electrochemical impedance behavior. Two distinct characteristic features can be noticed depending on the frequency: at high frequencies, it is in the form of a semicircle and, at low frequencies, it is a straight line at an angle to the real axis representative of diffusion phenomenon. The behavior is similar for different immersion times although the corrosion resistance is noticed to decrease after extended exposure to the salt solution. Such behavior is presumably due to surface porosity and surface roughness of the coating. As the frequency decreases, degree of penetration into pores increases with pore length being the determining factor for the maximum possible penetration depth. The values of the real and imaginary components of the area-impedance at 10 mHz, for 1 day immersion, are almost the same at 0.1 Hz after 14 days of immersion in the salt solution, implying changes in pore characteristics upon prolonged exposure to saline water. The corrosion behavior of the high-P coating (sample 2) is found to be inferior to that of medium-P coating (sample 1) as manifested by smaller diameters of the semicircles (Fig. 7b). The coating progressively degrades with longer immersion times showing linear behavior at lower frequencies upon immersion for 28 days.

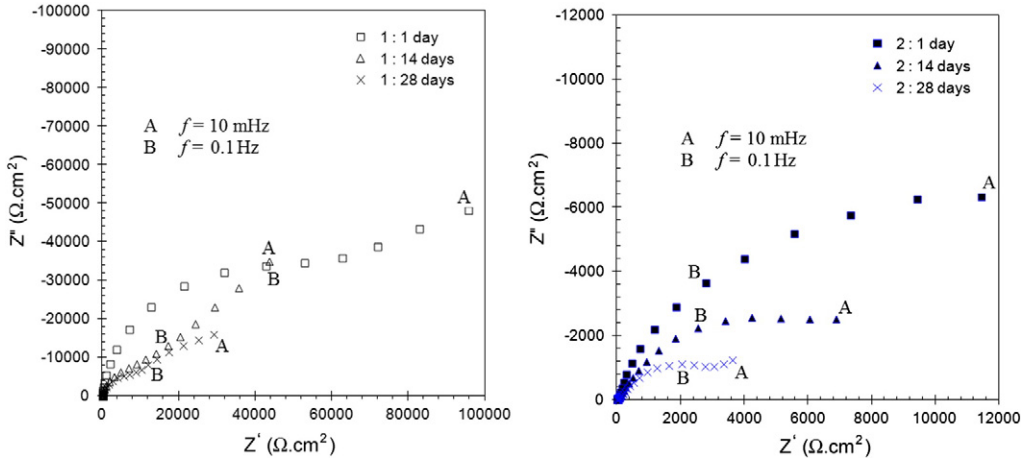

Fig. 7. Nyquist plots for pure Ni–P coatings (samples 1 and 2) from different immersion times in 4 wt.% NaCl solution.

The superior corrosion resistance of pure Ni–P coating with less P content (i.e. 10.8 wt.%P) led to the investigation of nanocomposite Ni–P–SiO_2 compositions obtained with 1 and 2 g/L SiO_2 loadings in the bath. Fig. 8 presents Bode diagrams for Ni–P–SiO_2 coatings (samples 3 and 4) after 1 and 14 days of immersion in the 4 wt.% NaCl solution. While the area impedance of sample 3 is less than that of sample 4 by several orders of magnitude after 1 day immersion suggesting less effectiveness of SiO_2 nanoparticles towards corrosion inhibition, the corrosion resistance is noticed to increase and become equivalent for both coating compositions after prolonged exposure of 14 days. It is speculated that extended exposure to the saline solution causes preferential nickel dissolution with subsequent appearance of embedded SiO_2 nanoparticles on the surface, hence increasing the degree of surface passivation. In addition to a significant increase in area-impedance, the drop in these values over the tested range of frequencies is less dramatic than that observed for pure Ni–P coatings. Such behavior may be attributed to improvements in the nanocoating characteristics (less surface roughness, elimination/minimization of surface porosity, etc.) during deposition as well as a passive layer formation due to phosphorus enrichment with little or no access of the electrolyte to the coating defects or the underlying substrate [10,12,32].

The Nyquist plots show only one semicircle indicative of single time constant. For sample 3, the corrosion resistance is very low after 1 day of immersion (Fig. 9a). The sample 4 (Fig. 9c), on the other hand, initially exhibits a semicircle after one day of immersion. The corrosion resistance is maximum after 14 days immersion, showing a semicircle with the maximum diameter and a straight line at lower frequencies. The latter may be indicative of an onset of electrolyte penetration through voids or pores to either the pre-coat Ni–P layer or the copper substrate surface. The SEM examination (Fig. 4c) corroborates this finding by showing microcracks that are sub-100 nm wide and a few tens of nanometers long. Further investigations are warranted to develop a theoretical fit of such corrosion behavior.

Corrosion behavior of the Ni–P and Ni–P–SiO_2 coatings can be described in terms of a theoretical fit using open-circuit potential (OCP), charge transfer resistance also known as coating resistance (R_{ct}) and double layer capacitance (C_{dl}). Although R_{ct} and C_{dl} have units of Ω cm^2 and F cm^{-2}, respectively, they are referred to as charge transfer resistance and double-layer capacitance, in line with reported works. When the electrode is polarized, i.e. an electrode potential is forced away from its value at open-circuit, the charge transfer resistance, also known as polarization resistance (R_p), arises either from kinetics of the reactions or the diffusion of the reactants towards and away from the electrode surface or both. The double layer capacitance (C_{dl}) is due to an electrical double layer formation between an electrode and its surrounding electrolyte owing to the adsorption of ions from the solution to the electrode surface and has a typical thickness value on the order of a few angstroms.

The values of OCP, R_{ct} and C_{dl} for different coatings are listed in Table 2. A drop in OCP values implies superior corrosion resistance in the absence of applied voltage. The R_{ct} values are indicative of the corrosion protectionability of a surface and generally, higher values imply superior corrosion resistance. In our case, the R_{ct} values are in the range of 10^4 Ω cm^2 but increase by about four orders of magnitude in case of SiO_2 nanoparticles incorporation (sample 4). Similarly, the C_{dl} value is related to the porosity level in the coatings with low values representing samples having less porosity. The elimination of surface porosity in the nanocomposites due to the addition of SiO_2 nanoparticles is confirmed from change in C_{dl} values that drop from ~10^{-5} for high-P Ni–P (sample 2) to 10^{-10} F cm^{-2} for Ni–P–SiO_2 (sample 4). It is, however, noteworthy that among different categories of Ni–P coatings,

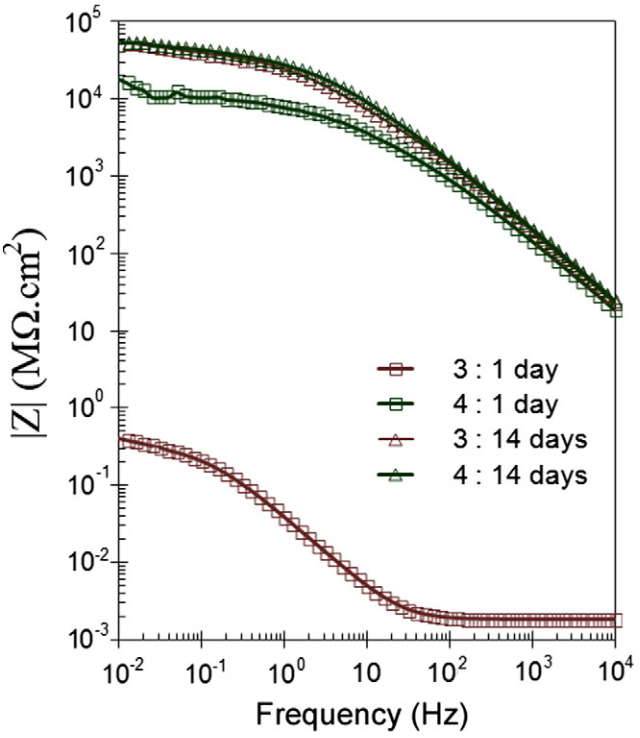

Fig. 8. Bode plots for nanocomposite Ni–P coatings (samples 3 and 4) after 1 and 14 days of immersion in 4 wt.% NaCl solution.

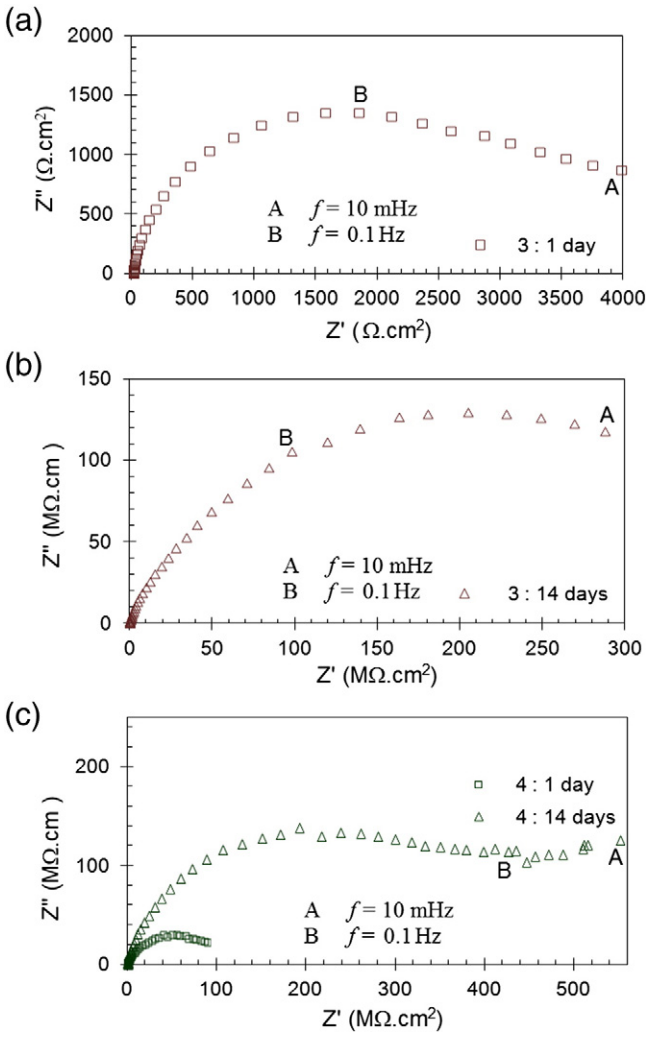

Fig. 9. Nyquist plots for Ni–P–SiO_2 nanocomposite coatings produced with SiO_2 bath loading of: (a, b) 1 g/L (Sample 3) and (c) 2 g/L (Sample 4).

Table 2
Corrosion properties of pure and nanocomposite coatings at 24 °C after different immersion times in 4 wt.% NaCl solution.

Sample ID	Days	$\|Z\|_{10\ mHz}$ (Ω cm^2)	OCP (mV vs. Ag/AgCl)	C_{dl} (F/cm^2)	R_{ct} (Ω cm^2)
1.	1	6.85×10^4	−278	2.37×10^{-6}	8.45×10^5
	14	5.19×10^4			
	28	2.12×10^4			
2.	1	1.58×10^4	−310	1.79×10^{-5}	6.77×10^4
	14	1.00×10^4			
	28	4.61×10^3			
3.	1	4.24×10^3	−84	1.42×10^{-10}	2.74×10^8
	14	5.54×10^8			
4.	1	2.25×10^8	−124	1.18×10^{-10}	3.14×10^8
	14	5.66×10^8			

high-P coatings offer superior corrosion characteristics due to their amorphous structure and less susceptibility to pitting with resultant more noble and passive polarization potential [33].

It is speculated that initial preferential dissolution of nickel causes coating surface enrichment with phosphorus followed by reaction with water to form an adsorbed layer of hypophosphite anions $(H_2PO_2)^-$ that surface passivates by blocking transport of water molecules to the electrode surface [34]. The influence of SiO_2 nanoparticles on further improvement in corrosion resistance of the nanocomposite coatings in saline water may be attributed to two factors namely: (i) modified microstructure promoting inhibition of defect corrosion by acting as inert physical barrier and (ii) uniform SiO_2 dispersion in Ni–P matrix causing formation of many corrosion micro-cells in which SiO_2 nanoparticle and nickel metal act as cathode and anode, respectively, due to more positive potential of SiO_2 than nickel and subsequent occurrence of homogeneous corrosion instead of localized corrosion.

4. Conclusions

By tuning the amount of NaH_2PO_2 (15 or 30 g/L) used as reducing agent in the precursor bath, the P-content in the Ni–P coatings can be controlled to produce medium- and high-P Ni–P. In the latter case, an increase in P weight percent is accompanied with an increase in the grain size and surface roughness. The addition of SiO_2 nanoparticles in the Ni–P matrix refines the grain size, lowers the degree of surface roughness and enhances coating density through reduction in surface porosity along with an increase in the hardness value. The maximum improvement in hardness to a value of ~11 GPa is observed in Ni–P–SiO_2 nanocoatings with medium-P that may be considered to be due to hindrance to dislocation movement offered by the SiO_2 nanoparticles in the ductile matrix. EIS studies after immersion of coatings in the 4 wt.% NaCl solution for 2 to 4 weeks indicate superior corrosion resistance offered by the medium-P coatings and a further improvement by orders of magnitude upon SiO_2 incorporation. The theoretical fit of the EIS data indicates a combination of very low double layer capacitance (C_{dl}) and very high charge transfer resistance (R_{ct}) that confirm reduced levels of surface porosity and improved corrosion protectionability of the Ni–P–SiO_2 nanocomposite coatings.

Acknowledgements

The authors gratefully acknowledge the technical and financial support of the Research Center of College of Engineering, Deanship of Scientific Research, King Saud University.

References

[1] C.K. Lee, Surf. Coat. Technol. 202 (2008) 4868.
[2] C. Sun, S.A. Baig, Z. Lou, J. Zhou, Z. Wang, X. Li, J. Wu, Y. Zang, X. Xu, Appl. Catal. B Environ. 158–58 (2014) 38.
[3] Y.S. Huang, F.Z. Cui, Surf. Coat. Technol. 201 (2007) 5416.
[4] V.K. Bulasara, O. Chandrashekar, R. Uppaluri, Chem. Eng. Res. Des. 89 (2011) 2485.
[5] J. Li, Y. Tian, Z. Huang, X. Zhang, Appl. Surf. Sci. 252 (2006) 2839.
[6] W.L. Liu, S.H. Hsieh, T.K. Tsai, W.J. Chen, S.S. Wu, Thin Solid Films 510 (2006) 102.
[7] L.-C. Kuo, Yu-C. Huang, C.-L. Lee, Y.-W. Yen, Electrochim. Acta 52 (2006) 353.
[8] So-Y. Cheon, So-Y. Park, Y.-M. Rhym, D.-H. Kim, J. Ho Lee, Curr. Appl. Phys. 11 (2011) 790.
[9] M. Islam, M.R. Azhar, N. Fredj, T.D. Burleigh, Surf. Coat. Technol. 236 (2013) 262.
[10] P.H. Lo, W.T. Tsai, J.T. Lee, M.P. Hung, Surf. Coat. Technol. 67 (1994) 27.
[11] C.T.J. Low, R.G.A. Wills, F.C. Walsh, Surf. Coat. Technol. 201 (2006) 371.
[12] M. Alishahi, S.M. Monirvaghefi, A. Saatchi, S.M. Hosseini, Appl. Surf. Sci. 258 (2012) 2439.
[13] S. Alirezaei, S.M. Monirvaghefi, A. Saatchi, M. Urgen, K. Kazmanlı, Tribol. Int. 62 (2013) 110.
[14] J. Novakovic, P. Vassiliou, Electrochim. Acta 54 (2009) 2499.
[15] K. Zielińska, A. Stankiewicz, I. Szczygieł, J. Colloid Interface Sci. 377 (1) (2012) 362.
[16] F. Bratu, L. Benea, J.-P. Celis, Surf. Coat. Technol. 201 (2007) 6940.
[17] L. Benea, E. Danaila, J.-P. Celis, Mater. Sci. Eng. A 610 (2014) 106.
[18] F.C. Walsh, C.P. de Leon, Trans. Inst. Met. Finish. 92 (2) (2014) 83.
[19] H.D. Ackler, R.H. French, Y.-M. Chiang, J. Colloid Interface Sci. 179 (1996) 460.
[20] Y. de Hazan, D. Zimmermann, M. Z'Graggen, S. Roos, C. Aneziris, H. Bollier, et al., Surf. Coat. Technol. 204 (2010) 3464.
[21] D. Dong, X.H. Chen, W.T. Xiao, G.B. Yang, P.Y. Zhang, Appl. Surf. Sci. 255 (2009) 7051.
[22] D. Gutsev, M. Antonov, I. Hussainova, A.Y. Grigoriev, Tribol. Int. 65 (2013) 295.
[23] S. Sadreddini, A. Afshar, Appl. Surf. Sci. 303 (2014) 125.
[24] T. Rabizadeh, S.R. Allahkaram, Mater. Des. 32 (2011) 133.
[25] F.C. Walsh, C.P. de León, C. Kerr, S. Court, B.D. Barker, Surf. Coat. Technol. 202 (2008) 5092.
[26] H.-M. Wu, W.J. Tseng, Ceram. Int. 41 (2015) 1863–1868.
[27] S.L. Zhu, L. Tang, Z.D. Cui, Q. Wei, X.J. Yang, Surf. Coat. Technol. 205 (2011) 2985–2988.
[28] S. Okada, T. Kamegawa, K. Mori, H. Yamashita, Catal. Today 185 (2012) 109–112.
[29] L. Benea, E. Danaila, J.-P. Celis, Mater. Sci. Eng. A 610 (2014) 106–115.
[30] J.Y. Song, Jin Yu, Thin Solid Films 415 (2002) 167.
[31] J.F. Shackelford, W. Alexander, Materials Science and Engineering Handbook, CRC Press LLC, Boca Raton, 2001. 474.
[32] A. Lasia, in: B.E. Conway, J. Bockris, R.E. White (Eds.), vol. 32, Kluwer Academic/Plenum Publishers, New York, 1999, pp. 143–248.
[33] R. Weil, K. Parker, in: G.O. Mallory, J.B. Hajdu (Eds.), Electroless Plating: Fundamentals and Applications, Noyes Publications/William Andrew Publishing, NY1990.
[34] E.T. van Der Kouwe, Electrochim. Acta 38 (14) (1993) 2093–2097.